Enclosure 3.

Preprint "Speckle Interferometry of Asteroids. III.

511 Davida."

SPECKLE INTERFEROMETRY OF ASTEROIDS

III. 511 Davida

J. D. Drummond and E. K. Hege

Steward Observatory

University of Arizona

Tucson, Arizona 85721

Running title: Interferometry of Davida

Send proofs to: J. D. Drummond
Steward Observatory
University of Arizona
Tucson, Arizona 85721

Submitted to Icarus 21 May 1985

36 manuscript pages
6 figures
9 tables

ABSTRACT

511 Davida was observed with the technique of speckle interferometry at Steward Observatory's 2.3m telescope on May 3, 1982. Based on 5 ten minute observations, its dimensions were found to be (465 $\pm$ 33) x (358 $\pm$ 39) x (258 $\pm$ 52) km. Such a shape falls close to an equilibrium figure of a "rubble pile," suggesting a density of 1.4 $\pm$ Ø.4 gm/cm^3. Simultaneous with the determination of the size and shape of Davida, we find its north pole to lie within 26^o of RA = 19^{h}Ø8^m, Dec = 15^o (λ= 291 ^{o}, β = +37^o).

We derive and apply to Davida a new simultaneous amplitude magnitude (SAM) aspect method for finding, from photometric data only, axial ratios and rotational pole coordinates. We also employ various weightings in a linear form of the amplitude aspect relation to find axial ratios and a pole. Precise albedos follow from speckle and photometry, but they depend on the form of the phase function (the Gehrels and Tedesco or Lumme and Bowell treatments) and the photometric method used to find the pole and axial ratios.

An alternative interpretation of the photometric data which cannot be excluded, is that rather than suggesting a change to the axial ratios found from speckle observations, the photometry could indicate albedo structure over the surface of Davida. The precision of our present autocorrelation/power spectrum result does not force a choice between a uniform albedo or an albedo gradient. Image reconstruction techniques presently under

development may, however, permit such discriminations.

Introduction

In order to find its triaxial dimensions and the direction of its angular momentum vector (its spin axis) we have obtained five speckle interferometric observations of the sixth largest (Zellner, 1979) minor planet, 511 Davida. Zappala and Knezevic (1985) have applied the amplitude-magnitude-aspect relationship (Zappala et al. 1983; Zappala and Knezevic 1984) to lightcurves of Davida extending back to 1952. We, too, derive and apply a new simultaneous amplitude-magnitude-aspect, and a weighted amplitude-aspect, method to the photometric data of Davida. These photometric methods lead to an independent check of the location of Davida's spin axis and its axial ratios as found through speckle interferometry, which, being a high angular resolution technique, follows the changing projected size, shape, and orientation of the asteroid to derive its pole and dimensions.

For image modelling purposes, an asteroid is assumed to be a triaxial ellipsoid rotating about its shortest axis ($a \geq b \geq c$), smooth (no large craters, mountains, etc.), featureless (no albedo variations), and uniformly bright (scatters geometrically). Such an ellipsoidal model asteroid projects as an apparent ellipse of uniform brightness on the plane of the Earth's sky. The two-dimensional image autocorrelation function of a uniformly bright ellipse has the same shape and orientation (but twice the size) as the ellipse itself. The corresponding image power spectrum also has the same elliptical shape, but

appears rotated 90° because of the reciprocal relation between image extent and spatial frequency. The projected figure of the real asteroid on the plane of the Earth's sky is thus characterized by the fit of an elliptical model to the observed image autocorrelation function or image power spectrum data. This yields the observed major axis dimension (α), minor axis dimension (β), and position angle of the major axis (γ) for a particular time in the asteroid's rotational cycle. The equations relating the observed elliptical parameters (α, β, γ) for a series of rotational phase angles, Ψ, to the three axes dimensions and pole direction of the triaxial ellipsoid are given by Drummond et al. (1985a). Thus, a non-linear least squares routine is applied to a series of (α, β, γ) and yields simultaneously six parameters: the three axes dimensions, two Euler angles (θ, the sub-Earth point latitude, and ψ_o, the zero point in the rotational cycle) and the obliquity (ρ, the projected angle between the asteroid's north pole and the ecliptic north pole; see Appendix I of Drummond et al. 1985a).

Observations and Results

On May 3, 1982, with the 2.3m telescope of Steward Observatory and the speckle camera and equipment described by Hege et al. (1982), five ten-minute speckle observations of Davida were made, each observation being preceded by an observation of one nearby star, and followed by another observation of a second star. The co-added power spectra of Davida for each ten minutes were divided by the power spectra of the flanking stars in order to remove the telescope modulation transfer function and the seeing (Hege et al. 1982; Drummond et al. 1985a,b). The aspect data for Davida on May 3, 1982, is given in Table I.

Table II gives the six parameter fit to the fifteen equations of condition (five α's, five β's, and five γ's). As for most non-linear least squares routines, our program (adopted from Jefferys 1980, 1981) linearizes about the residuals. The errors for the parameters can then be computed directly during the solution of the equations of condition. For 433 Eros (Drummond et al. 1985a) and 532 Herculina (Drummond et al. 1985b), the errors so computed appear to be reasonable. However for Davida they are unreasonably large, especially for the smallest dimension, c, because at certain orientations of the asteroid, the residual space (or χ-squared hyperspace) is quite convoluted and even discontinuous. As explained by Drummond et al. (1985a), at certain configurations the asteroid will appear

to suddenly reverse directions as it rotates. Near this configuration a small change in any of the six parameters during the iterations will result in a large change in the predicted position angles, and thus in the residuals. The errors computed in such a situation are not realistic. For instance, the minimum in the χ-squared hyperspace results in the solution that appears in Table II, but the formal error for c of $\pm$306 km implies that our data allows c to be negative.

Since this unphysical possibility is caused by the warped residual space, we compute the errors, instead, by considering the five solution sets of observations taken four at a time. For each of the six parameters we find the mean (μ) and standard deviation (δ) of the five sets, and calculate the error (σ) of p (the parameter solution given in Table II) by $\sigma^2 = (p-\mu)^2 + \delta^2$. (For two of the five sets only a 5 parameter fit [b=c] converged to a solution.)

Table III gives the 5 parameter solution, the prolate spheroid case (b=c) using all five observations. Since this biaxial ellipsoid never reverses direction of rotation, the χ-squared hyperspace is not warped, and there are no problems finding the solutions or computing the errors. However, the fit to α, β, and γ (none illustrated), are much worse than the triaxial case, and, furthermore, the triaxial solution does not allow a biaxial situation $(b - \sigma_b) > (c + \sigma_c)$. Therefore, unlike our treatment of Eros and Herculina, we do not consider a weighted average between the biaxial and triaxial solutions, and only use the latter (Table II), rejecting the biaxial solution

(Table III).

Fig 1
Fig 2
Fig 3

In Figure 1 we show the measured α's (upper filled circles) and β's (lower open circles), as a function of rotational phase. The upper line is the predicted α from the solution in Table II, and the lower line is the predicted β. Figure 2 shows the measured (circles) and predicted (line) γ's for our triaxial solution of Table II. To illustrate the problem caused by the weird shape of the residual space, Figure 3 results from using the adopted solution of Table II, but changing the latitude of the sub-Earth point, θ, by 1° from -39°.6 to -40°.6. In Figure 2 $\cos^2\theta > (a^2-b^2)/(a^2-c^2)$ and the condition for rotation reversal of the projected ellipse is satisfied. In Figure 3 $\cos^2\theta < (a^2-b^2)/(a^2-c^2)$ and the ellipse does not reverse directions.

Davida as a Rubble Pile

A particular sub-set of triaxial ellipsoid figures is allowed if a body is in hydrostatic as well as gravitational equilibrium. The shape of such objects is maintained by gravity only since they have no internal strength (Chandrasekhar 1969; Weidenschilling 1981). If an asteroid suffers a catastrophic collision it is possible that reaccumulation could occur among the ejecta with relative velocities less than the escape velocity of the largest remnant (Zappala et al. 1984). Such rubble piles (Davis et al. 1979) would form a particular triaxial ellipsoid equilibrium figure that is a function only of its angular momentum.

Within the errors, our determination of the shape of Davida suggests the possibility that it could be such an equilibrium figure, and since we know its volume and rotation period, it is possible to find its mean density as was suggested by Farinella et al. (1981). Following their lead, we note that for the equilibrium figure of 465x377x244, which falls within the errors of our observations, and has the same long dimension and volume as the solution from Table II, a rotational period of 5.1297 hours (Zappala and Knezevic, 1985) leads to a mean density of 1.4 $\pm$ 0.4 gm/cm^3. This density is rather low and could mean that there is substantial void space within the asteroid, or for that matter, may suggest that Davida is not a rubble pile after all.

Photometry

When the solar phase angle (ω) is less than substantial, there is a two-fold ambiguity in determining the pole direction from the changing size, shape, and orientation of the projected ellipses. However, this θ, $\pi-\theta$ ambiguity (Drummond et al. 1985a) which is manifest as a choice between two obliquities, and therefore two poles, can easily be resolved by considering lightcurve data. In Table IV we compare the observed lightcurve amplitudes (taken from Zappala and Knezevic, 1985 and from Vesely and Taylor, 1985) to our predicted amplitudes using pole 1 in Table II. The RMS deviation from the observed amplitudes is .04 mag, whereas with pole 2 it was found to be .18 mag. The choice between the two pole solutions is obvious.

Next we derive and apply yet another magnitude-amplitude-aspect relation. Several versions of the principle are currently used, e.g., Zappala's amplitude-magnitude (AM; Zappala et al. 1983, Zappala and Knezevic 1984), or Tedesco and Taylor's (1985) magnitude-amplitude-shape-aspect (MASA), relationships. To distinguish our new technique we dub our method the simultaneous amplitude-magnitude (SAM) relation. Adopting the assumptions from the introduction of this paper, the square of the amplitude (converted from magnitudes to a linear scale) of an asteroid's lightcurve is given as the ratio of maximum to minimum projected area squared

$$R^2 = (A + B \cos^2\theta)/(A + C \cos^2\theta) \qquad (1)$$

where $A = a^2b^2$, $B = a^2c^2 - a^2b^2$, and $C = b^2c^2 - a^2b^2$. The latitude of the sub Earth point, θ, comes from

$$\sin\theta = -[\cos(\lambda-\lambda_p)\cos\delta\cos\delta_p + \sin\delta\sin\delta_p],$$

where λ, δ and λ_p, δ_p are the known celestial or ecliptic coordinates of the asteroid and the unknown coordinates of the asteroid's pole, respectively.

Unlike photometric astrometry (Taylor and Tedesco, 1983), which takes advantage of the movement of the sub-Earth point across lines of longitude on the asteroid to derive a pole direction, the amplitude-magnitude-aspect relation, which takes advantage of the movement of the sub-Earth point across lines of latitude on the asteroid, is model-dependent in that it is a function not only of the location of the pole but of the axial ratios as well. Thus a non-linear least squares solution of equation (1) for ab, ac, bc, λp, and δp, (or A, B, C, λp, and δp) would result in finding simultaneously $a^2/b^2 = (A+B)/(A+C)$, $b^2/c^2 = A/(A+B)$, and $a^2/c^2 = A/(A+C)$ and λ_p, δ_p. A separate solution of the numerator in (1), using $V_o(1,\emptyset)$ converted to intensity (the magnitude-aspect relation), would yield only $b^2/c^2 = A/(A+B)$ and a pole position, if the amplitudes are not available. Thus two separate determinations of b^2/c^2 and the pole are made with eq. (1) and the magnitude-aspect method.

Another way of attacking the problem is to use a grid of poles and axial ratios to find the combination that minimizes the residuals between observed and predicted amplitudes and maximum intensities. Our new method, however, uses a linear least squares technique to find the axial ratios from a grid of possible poles, thus eliminating the necessity of sampling a grid of axial ratios. First, if only amplitudes are considered, then

by manipulating (1) we can form a linear amplitude aspect relation

$$(R^2-1)^{-1} = k + \ell \tan^2\theta \qquad (2)$$

and solve for k and ℓ for each trial pole where $k = (A+C)/(B-C)$ and $\ell = A/(B-C)$, and thus $a^2/b^2 = (k+1)/k$, $b^2/c^2 = \ell/(k+1)$, and $a^2/c^2 = \ell/k$. The pole and the resulting k and ℓ that minimize the residuals between "observed" and predicted $(R^2-1)^{-1}$ is chosen as the best solution. The drawbacks to this method are that it is a non-linear relation between the observable quantity R and the independent variable θ, and that it gives more weight to observations at higher θ. However, (2) is the simplest statement of the amplitude-aspect relation.

If both V_o and an amplitude for a given epoch are provided then it is possible to convert the maximum and minimum light to intensities squared, X^2 and N^2, respectively. Two linear combinations of these quantities yield two equations to solve for three unknowns. Adding and subtracting the numerator and denominator in (1) yields

$$X^2 + N^2 = K + L \cos^2\theta \qquad (3)$$

$$X^2 - N^2 = M \cos^2\theta \qquad (4)$$

A linear least squares solution of these equations for each trial pole is made, and again the pole giving the lowest vector sum of the residuals in (3) and (4) is chosen. The corresponding K, L, and M give the axial-ratios:

$$\frac{a^2}{b^2} = \frac{K+L+M}{K+L-M} = \frac{A+B}{A+C}$$

$$\frac{a^2}{c^2} = \frac{K}{K+L-M} = \frac{A}{A+C}$$

$$\frac{b^2}{c^2} = \frac{K}{K+L+M} = \frac{A}{A+B}$$

The advantage of this amplitude magnitude aspect method is that a linear least squares estimate is made for the unknowns, which yield axial ratios for the pole giving the lowest residuals for all the available information simultaneously.

We now apply this new method (SAM) by selecting the seven amplitudes in Table IV for Davida that have a corresponding V_o in Table V, an accumulation of $V(1,\omega)$'s by Zappala and Knezevic (1985) and Vesely and Taylor (1985) from original sources contained therein. But first, we use all the $V(1,\omega)$'s in Table V to construct the standard solar phase function plot of $V(1,\omega)$ vs ω, and show this as Figure (4). Using the eight points observed at $\omega > 6.5^o$ we find $V(1,\omega) = 6.445(\pm.042) + .040(\pm.004)$. Using the opposition effect as formulated by Gehrels and Tedesco (1979), we then calculate the RMS deviation from the solid line in Figure (4) for all eleven points as 0.035 mag. If we choose the Lumme and Bowell (1981a,b; Bowell and Lumme 1979) phase function description, we derive $m(0) = 6.132(\pm.063)$ and $Q = 0.045(\pm.028)$ with an RMS scatter of 0.033 mag. Both methods describe the data adequately but we will proceed in our analysis by using the residuals from the Gehrels and Tedesco formulation.

Implicit in the standard phase plot, Figure (4), is that $b/c = 1$, that the maximum area does not change with Θ. But let us attribute the residuals in Figure 4 to differences in Θ at

various oppositions, and convert each residual to an intensity. Then using the seven residuals that have corresponding amplitudes in Table IV we can derive seven (X^2,N^2) pairs. The only data that is excluded is the 1962 amplitude for which a V_o was not found; also, only one amplitude and V_o from 1979 is chosen so as not to bias the results toward one opposition. Next we construct a grid of pole positions at 1^o intervals in both ecliptic longitude and latitude in the region of the poles found by speckle and by Zappala and Knezevic (1985).

We find solutions for our SAM method (equations (3) and (4)), and for the amplitude-aspect relation as given by (2). Bevington (1969) suggests that when a non-linear equation is transformed to a linear equation, the equations of condition should be weighted. In our case (2) should be weighted by $\left[\frac{d(R^2-1)^{-1}}{dR^2}\right]^{-2} = (R^2-1)^4$. This seems rather severe, so in addition to finding the unweighted least squares solution to (2), we also find two weighted solutions, one using the suggested $(R^2-1)^4$ as weights and one using $(R^2-1)^2$. Table VI gives the pole and axial ratios for the four methods, along with the errors as found by a formal analysis of the propagation of the uncertainties in the coefficients K, L, and M, or k and l, generated from the linear least squares routines. For instance the error in the a/c ratio using (2) is

$$\sigma_{a/c} = \frac{\partial a/c}{\partial a^2/c^2} = \frac{\partial (l/k)^{1/2}}{\partial (l/k)} \sigma_{l/k} = .5(a/c)^3 l^{-2} \left(k^2\sigma_l^2 + l^2\sigma_k^2\right)^{1/2}.$$

The RMS error for the location of the pole arises from the differences between the θ's calculated from the given pole and

from inverting (2):

$$\theta = \tan^{-1}\left[\frac{(R^2-1)^{-1}-k}{l}\right]^{1/2} = \tan^{-1}\left[\frac{c^2/b^2 - R^2c^2/a^2}{R^2-1}\right]^{1/2}$$

The RMS amplitudes (converted back to magnitude from intensities) arises from comparing the observed amplitudes to a rearranged (1)

$$R^2 = \frac{\frac{c^2}{b^2}\cos^2\theta + \sin^2\theta}{\frac{c^2}{a^2}\cos^2\theta + \sin^2\theta}$$

Rounding out Table VI are the equivalent results from the entirely independent method of speckle interferometry based on the May 3, 1982 observations. Note that the 8° RMS error for the speckle pole in Table VI is determined from photometric data, whereas the 26° uncertainty in Table II derives from speckle observations.

In Table VII we show the solar phase functions for each of the solutions in Table VI, using both the Gehrels and Tedesco phase function and the Lumme and Bowell formulation, although the residuals to the b/c = 1 phase function (Figure 4) were determined from the Gehrels and Tedesco fit for input into the SAM method. For the cases where $b/c \neq 1$, the observed $V(1,\omega,\theta)$'s were corrected to the polar view $V(1,\omega,90^\circ)$ using the appropriate b/c and pole.

Of the photometric solutions for the pole and axial ratios in Tables VI and VII, we prefer the results from the simultaneous-amplitude-magnitude method because it uses both V_o and amplitudes simultaneously and is a simple combination of linear equations. The vector sum of the RMS scatter in

magnitudes from the predicted and observed amplitudes from Table VI, column 7, and from the predicted and observed $V(1,\omega,\Theta)$ from Table VII, column 3, is ~~.036~~ .023 mag. ~~Nearly~~ Not as good is the amplitude-aspect relation (eq. 2) weighted by $(R^2-1)^2$, which gives a vector sum of RMS scatter of .Ø37. The unweighted amplitude-aspect method, and the amplitude-aspect method weighted by $(R^2-1)^4$, give RMS scatters of .Ø49 and .Ø96 magnitudes, respectively, and we do not consider them serious contenders for possible models of Davida. Figures 5 and 6 show the aspect corrected solar phase functions for the SAM results and for the preferred weighted amplitude aspect method (WAA), respectively, although the latter method uses only amplitudes as input and does not use V_o data at all.

Fig 5
Fig 6

Other salient points from this analysis of photometric data are 1) Regardless of the method, the a/b ratio seems to be well determined at 1.24. 2) The location of the pole is also well determined and is not very sensitive to the method. 3) On the other hand, the a/c and b/c ratios vary dramatically with the location of the pole and the method of analysis. 4) The uncertainties in the axial ratios increase with increased weighting. 5) The Lumme-Bowell formulation of the phase function appears to give slightly (but perhaps insignificantly) lower residuals in the fits to the data than the Gehrels and Tedesco method. 6) None of the axial ratios derived from photometry are equilibrium figures.

Combining Speckle and Photometry

One of the most useful applications of speckle and photometric data is in the derivation of rather precise albedos, especially for dark objects where the polarization slope-albedo law saturates (Dollfus and Zellner 1979). For each of the fits for Davida in Table VI we find the figure requiring the least change (in an RMS sense) in the speckle dimensions to meet the axial ratios found from the photometry. These dimensions are listed in Table VIII along with the uncertainties, where the latter are calculated as the vector sum of the uncertainty in the speckle dimension plus the difference between the speckle and photometric dimension. Also listed in the table are the visual albedos calculated with the V(1,Ø)'s and m(Ø)'s of Table VII according to eq. (3) of Dollfus and Zellner (1979), where the errors in the albedos follow from the propagation of the uncertainties in a, b, and V(1,Ø) or m(Ø).

Table VIII

Comparisons and Summaries

In one night, speckle interferometric observations yield a triaxial ellipsoid figure for Davida, and two pole solutions. A simple inspection of the lightcurve history of the asteroid easily distinguishes between the two. The pole lies within 26° of ecliptic coordinates (291°; +37°), and the axial ratios are a/b = 1.30 ± .17 and b/c = 1.39 ± .32. This compares favorably to Zappala and Knezevic's (1985) results from their amplitude-magnitude-aspect (AM) method, which give a pole some 10° from ours at (303°±4°; +34°±5°) or taking into account scattering, 12° away at (302°±6°; +29°±6°). Their axial ratios also agree with ours to within our errors: a/b = 1.26 and b/c = 1.18 (or 1.19 and 1.13 with scattering corrections).

We derive a new simultaneous amplitude-magnitude-aspect (SAM) technique that for Davida yields a pole within 2.°3 of (308°; +30°), 16° away from the speckle pole, and axial ratios of a/b = 1.24±.03, and b/c = 1.12±.03, both within the uncertainties of the values found from speckle. If only amplitudes are considered, then our version of a weighted amplitude-aspect relation gives a pole at (311°; +32°), with an uncertainty of 2.°6. The axial ratios for this method are a/b = 1.24±.09 and b/c = 1.24±.09.

Although Taylor (Vesely and Taylor, 1985) was not able to achieve a totally satisfactory result with photometric astrometry

of Davida, by considering only pairs of observations at the same longitudes a pole within 22° of (285°; +45°) was suggested, which is only 9° from the speckle pole. Chang and Chang (1963), from only four lightcurves, found a pole at (306°, + 34°) with an early version of the amplitude-aspect relation, superseding the one Gehrels and Owings (1962) found at (122°, +10°) from three lightcurves.

The radiometric diameter of Davida is listed as 323 km by Morrison and Zellner (1979) and 335 km by Bowell et al. (1979). The mean diameter from speckle $(abc)^{1/3}$ is 350 ± 28 km, from speckle and SAM is 361 ± 35 km, and from speckle and WAA is 359 ± 30 km, all in reasonable agreement.

The albedo computed for the speckle dimensions is p_v = 0.036 ± .005, or from either of our favored photometric models p_v = .033 ± .005 with the Gehrels and Tedesco phase function. With the Lumme and Bowell phase relation p_v is (0.041-.042)±(0.006-.007).

While the photometric SAM and WAA results for the pole and axial ratios are consistent with the results from speckle interferometry, in the sense that they fall within the tolerances of the speckle measurements, it is nevertheless tempting to try to explain the 16-17° difference between the speckle and photometric poles, and the differences between the axial ratios, because the speckle shape implies an equilibrium figure and the photometric ratios do not. (In this connection it should be noted that although neither the SAM nor any of the amplitude-aspect ratios are equilibrium figures, the mean of the two weighted methods, $A/A(R^2-1)^2$ and $A/A(R^2-1)^4$ in Table VI, are very close to the suggested equilibrium figure of 465x377x244.) It is

possible to reconcile the differences between the speckle and photometric results by invoking an albedo structure over the asteroid.

If the speckle rotational pole and axial ratios are considered correct, then a photometric pole some 16-17° away from the rotational pole implies that the brightest point on the asteroid is off-axis and would lead to asymmetric lightcurves. If the photometric ratios and pole are considered correct than the discrepancy in the speckle results is probably due to the fact that they are based on only 5 ten-minute observations at one aspect on one night, whereas the photometry was gathered over 28 years at various aspects. Between these two independent solutions are many possible albedo structures that would bridge the two results. For instance, with the speckle dimensions and the photometric rotational pole, the albedo structures listed in Table IX for both phase functions and each photometric method would produce exactly the photometric history of Davida. Thus for the SAM method, a 23% decrease in albedo from the view along the a axis to the view from over the pole, and a decrease of 5% from the view along the a axis to the view along the b axis, would produce, with the speckle dimensions and photometric pole, the same photometric behavior as would the SAM model in Tables VI-VIII. For the WAA results a decrease of 15% and 4%, respectively, would produce the same photometric history as the WAA model in Tables VI-VIII. While the photometric axial ratios in Table VI do not allow an equilibrium figure, the speckle dimensions, with or without the albedo structures given in Table

IX, do, of course, lead to the equilibrium figure density of 1.4 gm/cm^3.

With the photometric data available, then, there is no way to choose between a uniform albedo, non-equilibrium figure, and an equilibrium figure with albedo gradients. However, we are developing an image reconstruction program, which is the ideal use of speckle interferometric data, and perhaps a successful image reconstruction will shed light on the matter.

ACKNOWLEDGEMENTS

We thank Eugene Periman and Gary Schmidt for helpful discussions regarding the properties of least squares fitting procedures. This work is supported under NASA contract NAGW-224.

References

Birch, P. V., E. F. Tedesco, R. C. Taylor, R. P. Binzel, C. Blanco, S. Catalano, P. Hartigan, F. Scaltriti, D. J. Tholen, and V. Zappala (1983). Lightcurves and phase function of asteroid 44 Nysa during its 1979 apparition. Icarus 54, 1-12.

Bowell, E., T. Gehrels, and B. Zellner (1979). Magnitudes, colors, types, and adopted diameters of the asteroids. In Asteroids (T. Gehrels, Ed.) 1108-1129, University of Arizona Press, Tucson.

Bowell, E. and K. Lumme (1979). Colorimetry and magnitudes of asteroids. In Asteroids (T. Gehrels, Ed.) 132-169, University of Arizona Press, Tucson.

Chandrasekhar, S. (1969). Ellipsoidal Figures of Equilibrium. Yale University Press, New Haven, Conn./London.

Chang, Y. C., and C. Chang (1963). Photometric observations of variable asteroids. II. Acta Astron. Sin. 11, 139-149.

Davis, D. R., C. R. Chapman, R. Greenberg, S. J. Weidenschilling, and A. W. Harris (1979). Collisional evolution of asteroids: populations, rotation, and velocities. In Asteroids (T. Gehrels, Ed.) 528-557, University of Arizona Press, Tucson.

Dollfus, A. and B. Zellner (1979). Optical polarimetry of asteroids and laboratory samples. In Asteroids (T. Gehrels, Ed.) 170-183, University of Arizona Press, Tucson.

Drummond, J. D., W. J. Cocke, E. K. Hege, P. A. Strittmatter, and J. V. Lambert (1985a). Speckle interferometry of asteroids. I. 433 Eros. Icarus 61, 132-151.

Drummond, J. D., E. K. Hege, W. J. Cocke, J. D. Freeman, J. C. Christou, and R. P. Binzel (1985b). Speckle interferometry of asteroids. II. 532 Herculina. Icarus 61, 232-240.

Farinella, P., P. Paolicchi, E. F. Tedesco, and V. Zappala (1981). Triaxial equilibrium ellipsoids among the asteroids? Icarus 46, 114-123.

Gehrels, T. and D. Owings (1962). Photometric studies of asteroids. IX. Additional lightcurves. Astrophys. J. 135, 906-924.

Gehrels, T. and E. F. Tedesco (1979). Minor planets and related objects. XXVIII. Asteroid magnitudes and phase relations. Astron. J. 84, 1079-1087.

Hege, E. K., E. N. Hubbard, P. A. Strittmatter, and W. J. Cocke (1982). The Steward Observatory speckle interferometry system. Optica Acta 29, 701-715.

Jeffreys, W. H. (1980). On the method of least squares. Astron. J. 85, 177-181.

Jeffreys, W. H. (1981). On the method of least squares. II. Astron. J. 86, 149-155.

Lumme, K. and E. Bowell (1981a). Radiative transfer in the surfaces of atmosphereless bodies. I. Theory. Astron. J. 86, 1694-1704.

Lumme, K. and E. Bowell (1981b). Radiative transfer in the surfaces of atmosphereless bodies. II. Interpretation of

phase curves. Astron. J. 86, 1705-1721.

Morrison, D. and B. Zellner (1979). Polarimetry and radiometry of the asteroids. In Asteroids (T. Gehrels, Ed.) 1090-1097, University of Arizona Press, Tucson.

Taylor, R. C. (1979). Pole orientations of asteroids. In Asteroids (T. Gehrels, Ed.) 480-493, University of Arizona Press, Tucson.

Taylor, R. C. and E. F. Tedesco (1983). Pole orientation of asteroid 44 Nysa via photometric astrometry, including a discussion of the method's application and its limitations. Icarus 54, 13-22.

Vesely, C. D. and R. C. Taylor (1985). A survey of asteroid lightcurves. Submitted to Icarus.

Weidenschilling, S. J. (1981). How fast can an asteroid spin? Icarus 46, 124-126.

Zappala, V., M. DiMartino, P. Farinella, and P. Paolicchi (1983). An analytical method for the determination of the rotational directions of asteroids. In Asteroids, Comets, Meteors (C. I. Lagerkvist and H. Rickman, Eds.) 73-76, Uppsala Universitet Repocentralen HSC, Uppsala.

Zappala, V. and Z. Knezevic (1984). Rotation axes of asteroids: Results for 14 objects. Icarus 59, 436-455.

Zappala, V. and Knezevic (1985). Pole coordinates of the asteroid 511 Davida via amplitude-magnitude method. In preparation.

Zappala, V., P. Farinella, Z. Knezevic, and P. Paolicchi (1984). Collisional origin of the asteroid families: Mass and velocity distributions. Icarus 59, 261-285.

TABLE I.

Aspect Data for Speckle Observations

Date	RA	Dec
3 May 1982	15^h56^m	-2° 08'

Distance from Earth	Distance from Sun
2.655 AU	3.604 AU

Solar Phase Angele	Position Angle of Sun centered on Davida
6°3	53°

TABLE II.

Triaxial Solution

a	=	465 ± 33 km
b	=	358 ± 39 km
c	=	258 ± 52 km
ψ_o	=	$-10° \pm 44°$
θ	=	$-40° \pm 28°$
ρ_1	=	$285° \pm 26°$
ρ_2	=	$105° \pm 26°$

Pole 1

RA = 19^h08^m Dec = +15°

Ecliptic Long = 291° Lat = +37°

Pole 2

RA = 12^h40^m Dec = -18°

Long = 196° Lat = -12°

The error radius around each pole solution is 26°.

TABLE III.

Rejected Biaxial Solution

a	=	512 ± 100 km
$b = c$	=	334 ± 39 km
ψ_o	=	$-24° \pm 14°$
θ	=	$-14° \pm 13°$
ρ_1	=	$324° \pm 17°$
ρ_2	=	$144° \pm 17°$

Pole 1

RA = 20^h56^m Dec = +16°

Ecliptic Long = 322° Lat = +32°

Pole 2

RA = 10^h52^m Dec = -17°

Long = 171° Lat = -23°

The error radius around each pole solution is 16°.

TABLE IV.

Amplitudes

Date	λ	β	Observed Amplitude	θ_1	Speckle Predicted Amplitude	O-C
Jan. 26, 1952	112	+3	0.06	+50	0.06	0.00
April 8, 1953	200	+22	.25	-12	.25	.00
Jan. 26, 1958	147	+12	.09	+30	.15	-.06
Dec. 5, 1962	63	-17	.12	+43	.09	.03
Dec. 30, 1968	100	-4	.07	+55	.05	.02
Mar. 21, 1970	195	+22	.22	-9	.27	-.05
Aug. 7, 1972	304	-7	.06	-44	.09	-.03
Dec. 6, 1979	52	-18	.18	+35	.13	.05

TABLE V.

$V(1,\omega,\theta)$

Date	λ	β	ω	$V(1,\omega)$	θ_1	Speckle $V(1,\omega, 90)$
Jan. 26, 1952	112	+3	5.0	6.55	+50	6.43
April 8, 1953	200	+22	6.6	6.72	-12	6.39
Jan. 26, 1958	147	+12	8.1	6.72	+30	6.48
Dec. 29/30, 1968	100	-4	1.65	6.35	+55	6.26
Mar. 21, 1970	195	+22	7.8	6.82	-9	6.48
Aug. 7, 1972	304	-7	3.6	6.48	-44	6.32
Oct. 31, 1979	60	-20	10.7	6.86	+43	6.70
Nov. 12, 1979	59	-20	7.9	6.73	+42	6.56
Dec. 7, 1979	52	-18	10.0	6.83	+35	6.62
Dec. 17, 1979	51	-17	12.8	6.96	+34	6.74
Jan. 3, 1980	50	-14	17.2	7.13	+31	6.89

Table VI. Pole and Axial Ratio Solutions

	Ecliptic Pole Coordinates λ	β	θ RMS	a/b	a/c	b/c	RMS Amplitudes (mag) (n=7)
Speckle	291	+37	8.0	1.30±.17	1.80±.39	1.39±.32	.044
SAM (eq. 3 & 4)	308	+30	2.3	1.24±.03	1.39±.07	1.12±.03	.011
Amplitude/Aspect$_2$ eq. 2; wt=$(R^2-1)^2$	311	+32	2.6	1.24±.09	1.54±.13	1.24±.09	.011
Amplitude/Aspect unweighted	309	+25	3.6	1.23±.04	1.17±.04	0.95±.02	.015
Amplitude/Aspect wt=$(R^2-1)^4$	316	+42	2.1	1.25±.11	2.20±.56	1.76±.44	.009

Table VII Phase Functions

	Gehrels and Tedesco			Lumme and Bowell		
	V(1,0,90)	Phase Coefficient	RMS Mag (n=11)	m(o)	Q	RMS Mag.
b/c=1	6.445 (±.042)	.040 (±.004)	.035	6.132 (±.063)	.045 (±.028)	.033
Speckle	6.177 (±.029)	.043 (±.003)	.059	6.030 (±.117)	.172 (±.047)	.057
SAM	6.353 (±.026)	.039 (±.002)	~~.034~~ .030	6.109 (±.041)	.116 (±.017)	.022
Amplitude/Aspect wt=$(R^2-1)^2$	6.295 (±.031)	.036 (±.003)	.035	6.084 (±.055)	.182 (±.022)	.029
Amplitude/Aspect unweighted	6.479 (±.052)	.041 (±.005)	.047	6.145 (±.076)	.018 (±.034)	.041
Amplitude/Aspect wt=$(R^2-1)^4$	6.046 (±.078)	.030 (±.007)	.096	5.930 (±.171)	.362 (±.070)	.072

Table VIII Diameters and Albedos

	a	b	c	p_V(G&T)	p_V(L&B)
Speckle	465±33	358±39	258±52	.036±.005	.041±.007
SAM	432±47	349±40	312±75	.033±.005	.042±.007
$A/A(R^2-1)^2$	445±39	358±39	291±62	.033±.005	.041±.006
A/A	409±65	332±47	349±105	.033±.007	.045±.010
$A/A(R^2-1)^4$	470±33	376±43	214±68	.038±.006	.042±.009

Table IX Orthogonal Albedos for Speckle Dimensions and Photometric Pole

Gehrels and Tedesco

	p_c	p_b	p_a
SAM	.030	.038	.039
$A/A(R^2-1)^2$	.032	.036	.038
A/A	.027	.039	.0042
$A/A(R^2-1)^4$	.040	.032	.033

Lumme and Bowell

	p_c	p_b	p_a
SAM	.038	.047	.049
$A/A(R^2-1)^2$	.039	.044	.046
A/A	.037	.054	.056
$A/A(R^2-1)^4$	.045	.035	.037

Figure Captions

Fig. 1. Measured major (α) and minor (β) axis dimensions (solid and open dots, respectively) as a function of rotational phase for 511 Davida on May 3, 1982. The upper line is the least squares fit to the major axis dimensions and the lower line in the simultaneous fit to the minor axis dimensions. Maximum area (maximum light) occurs at rotational phase 0° and 180°.

Fig. 2. Measured relative position angles (dots) of the major axis and the simultaneous (along with the data in Fig. 1) least squares fit to the measured position angles (γ) as a function of rotation on May 3, 1982. At rotational phase 0° and 180°, maximum area is reached, and $\underline{a}$ is perpendicular to our line of sight, lying unforeshortened in the plane of the Earth's sky. Note that the position angle reverses direction near minimum light at rotational phases -90° and 90°.

Fig. 3. Same as Fig. 2, but the latitude of the sub-Earth point (θ) has been changed by one degree. Unlike in Fig. 2, for this aspect the asteroid would not appear to reverse directions during rotation. The one degree change in θ results in a large change to the structure of the residuals. See text.

Fig. 4. Standard (b assumed equal to c) solar phase plot of V_o (from Table V) vs solar phase angle. The linear portion of the Gehrels and Tedesco phase function is calculated from the eight points observed at greater

than 6.5°. The intercept of this line is at $V_o(1,\emptyset)$ = 6.445, while the intercept for the Lumme and Bowell fit is $m(\mathcal{O})$ = 6.132. See Table VII.

Fig. 5. Solar phase function for the simultaneous-amplitude-magnitude (SAM) aspect results given in Tables VI and VII. Here the brightness $V(1,\omega,\Theta)$ is corrected to $V(1,\omega,90)$, the view from above the pole. The Gehrels and Tedesco phase function formulation is used and a line is fit to the eight points observed at greater than 6.5°.

Fig. 6. Same as Fig. 5, but for the weighted, by $(R^2-1)^2$, linear amplitude-aspect results. The line is a fit to the seven points observed at greater than 7°.

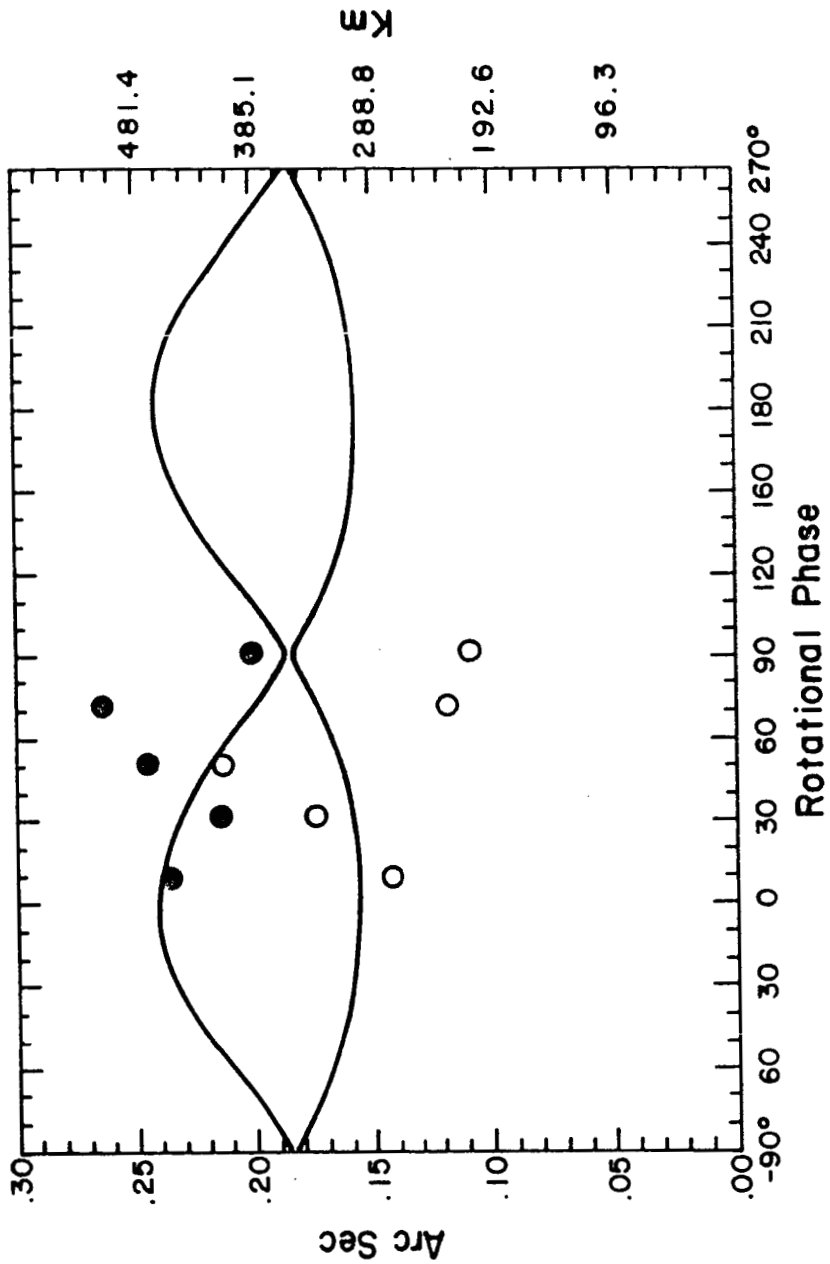

Fig 1
Drummond
&
Hege

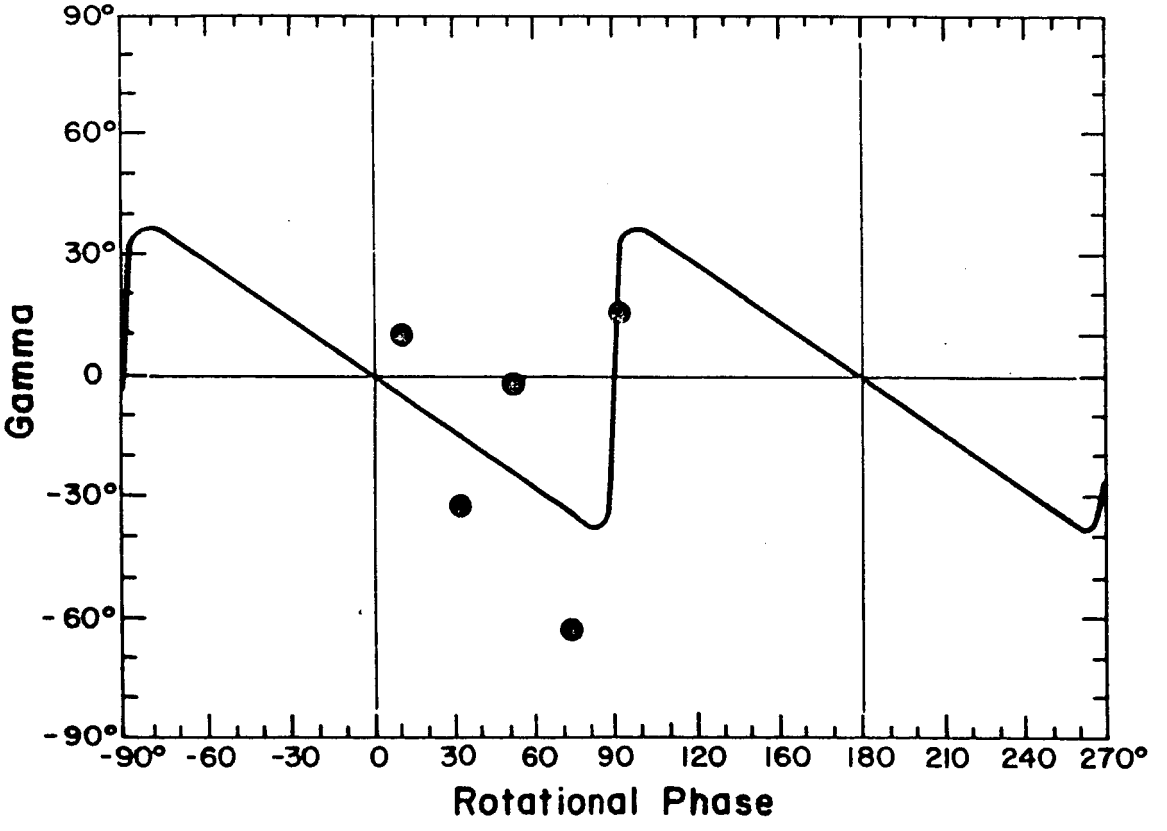

Fig 2
Drummond
Hagen

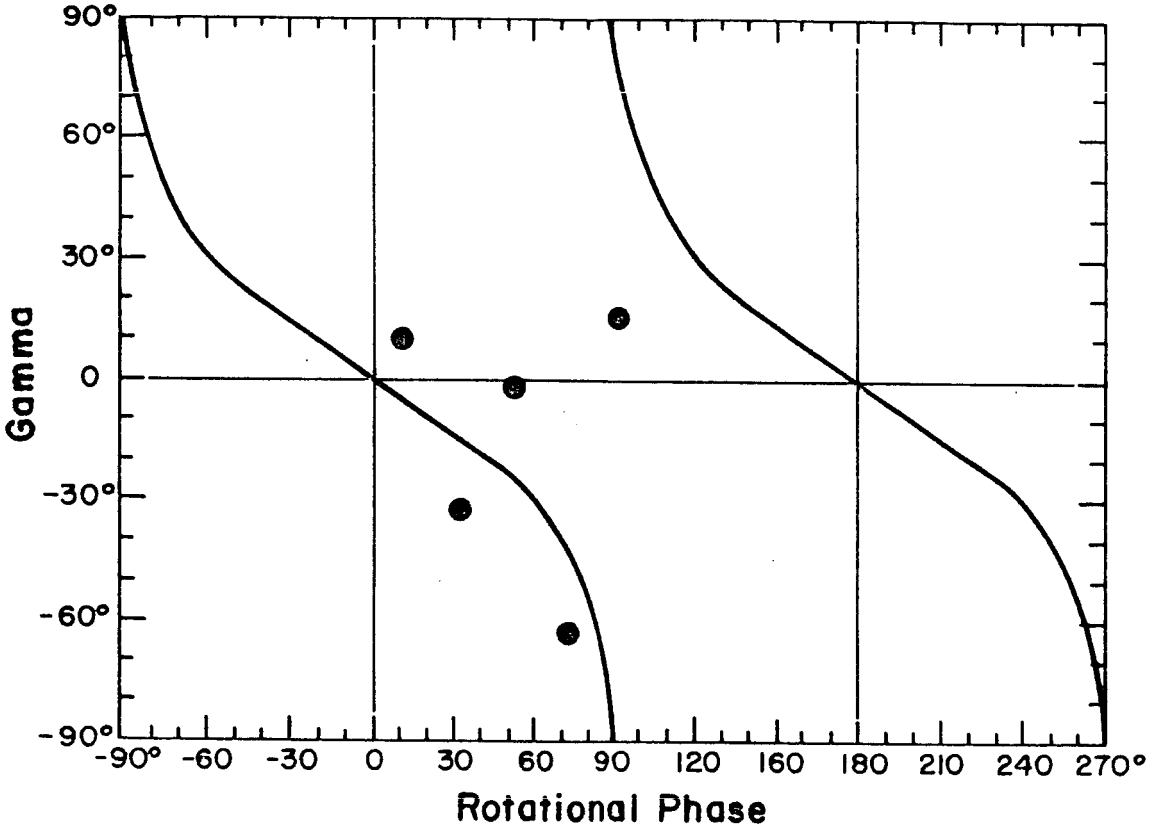

Fig 3
Diamond
p
1259

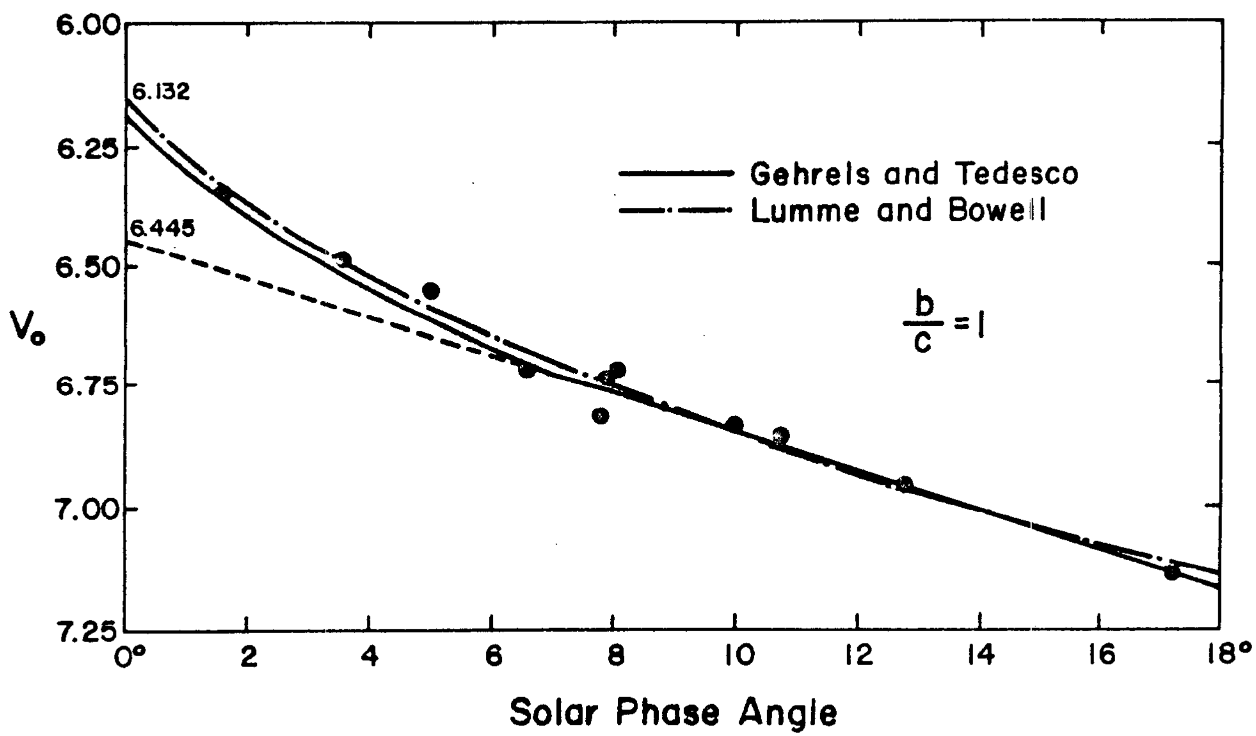
6.00
6.25
6.50
6.75
7.00
7.25
V_o
6.132
6.445
Gehrels and Tedesco
Lumme and Bowell
$\frac{b}{c} = 1$
0°
2
4
6
8
10
12
14
16
18°
Solar Phase Angle

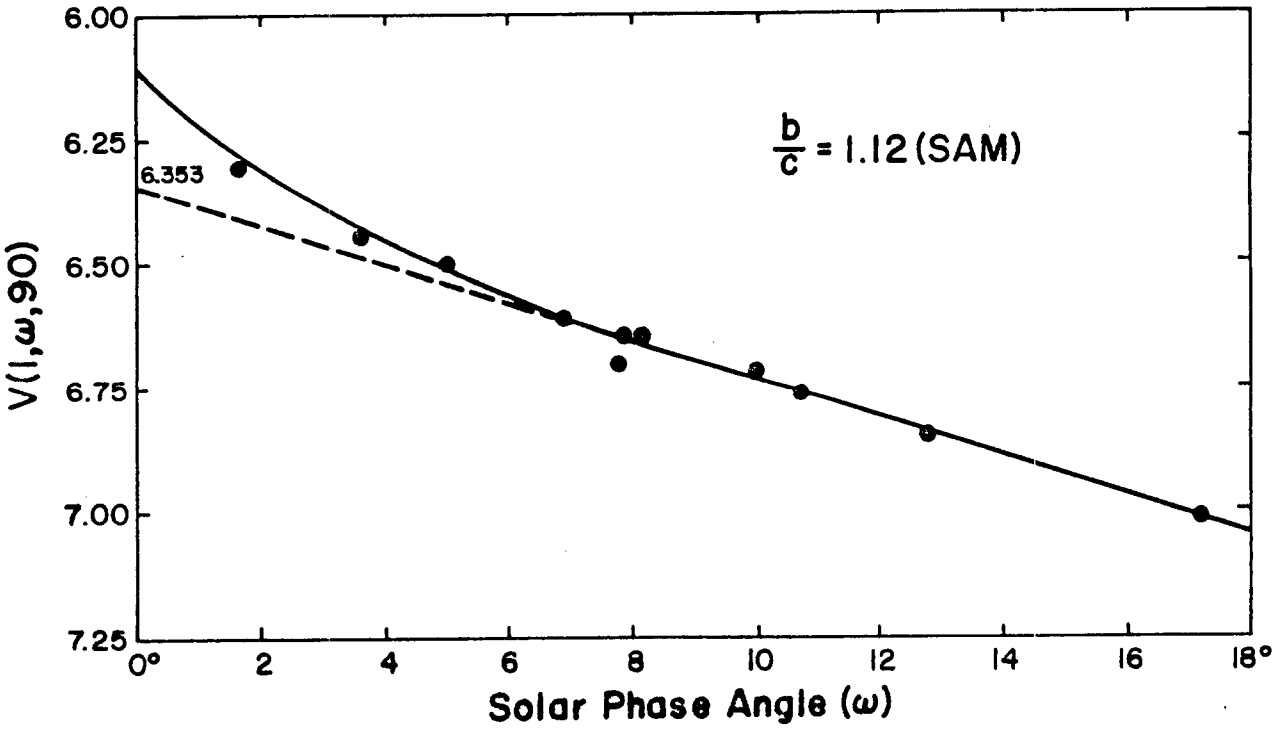
6.00
6.25
6.50
6.75
7.00
7.25
6.353
$\frac{b}{c}$ = 1.12 (SAM)
V(1,ω,90)
0°
2
4
6
8
10
12
14
16
18°
Solar Phase Angle (ω)

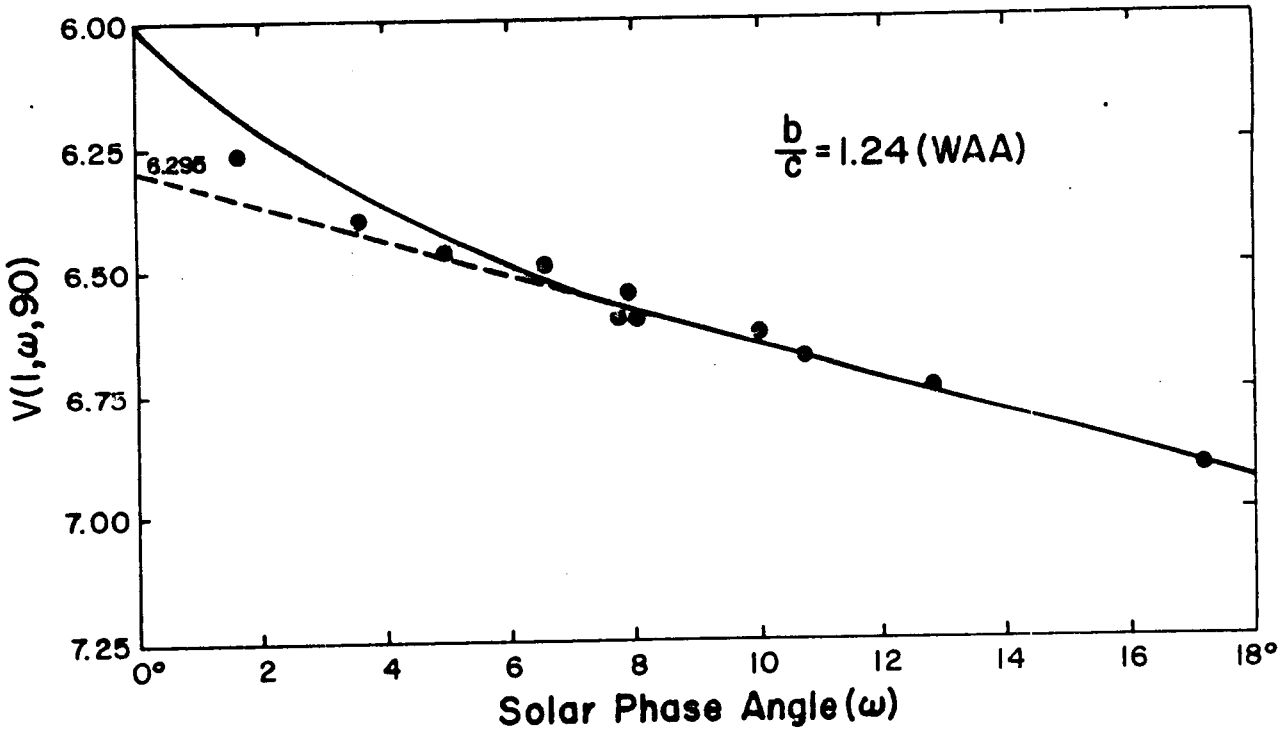
6.00
6.25
6.50
6.75
7.00
7.25
6.295
$\frac{b}{c}$ = 1.24 (WAA)
V(1,ω,90)
0°
2
4
6
8
10
12
14
16
18°
Solar Phase Angle (ω)